DOI: 10.1002/chem.201000393

T4 Virus-Based Toolkit for the Direct Synthesis and 3D Organization of Metal Quantum Particles

Li Hou, Faming Gao,* and Na Li[a]

Abstract: One of the challenges in building superstructures based on small metal particles is producing stable interparticle separation. Herein, we present a novel assembly method based on the use of the T4 bacteriophage capsid as a scaffold for the construction of 3D monodisperse metal–particle arrays. The highly regular and symmetrical protein surface of the T4 capsid allows the site-directed adsorption and subsequent reduction of metal ions, thus permitting the growth of metal particles in situ to enable them to exist at a quantum size with a high degree of monodispersity. Both these characteristics contribute to a great improvement in the electrocatalytic activity of the patterned noble-metal particles. Organized magnetic particles as small as 2–4 nm still maintain an observable ferromagnetic behavior, which makes them promising for a variety of possible biomedical applications.

Keywords: quantum dots · template synthesis · transition metals · viruses

Introduction

With an increasing requirement for versatile nanoparticle-based superstructures, there has been growing interest among chemists in the use of the structural specificity and strong interactions present in biology to control the synthesis of monodisperse metal particles with a defined size and shape and to direct these particles to assemble into one-, two-, or three-dimensional arrays.[1] Dujardin et al. used the 1D nature of the tobacco mosaic virus (TMV) to produce linear arrays of regularly spaced Ag nanoparticles.[2] Okuda et al. built 2D arrays of In nanoparticles by using a denatured-protein film method.[3] Besides the widely researched 1D or 2D complex structures, the 3D assembly of metal particles with a virus has also been predicted to be promising in a wide range of electronic devices.[4] However, reports on the biotemplate-directed assembly of 3D particle arrays are scarce.[5] Especially, the fabrication of such 3D metal/virus (M/V) structures with synthesized metal nanoparticles located with a high degree of monodispersity has not been achieved so far.

The way to solve this problem mainly depends on two major strategies: selection of a well-ordered 3D biological structure as a scaffold and careful manipulation of the specific metal ion or particle/surface interactions. Herein, we have tried to combine the T4 phage template with an approach to control the nucleation site to regulate the size of the particles and the sites at which they nucleate. Herein, the successful organization of a range of metal particles on the T4 capsid is presented, in which the 3D patterned metal particles are of quantum size (2.0–4.5 nm) with specific interparticle distances. Through these highly efficient manipulations on the 3D nanoscale, organized noble-metal nanoparticles can show a much higher electrocatalytic activity than the unsupported nanoparticles in CO-stripping measurements and organized magnetic particles as small as 2–4 nm can maintain observable ferromagnetic behavior, whereas magnetic particles smaller than 20 nm were commonly reported to be in the superparamagnetic regime.[6] It is worth noting that, in contrast to the cases reported previously,[7] we conducted the binding and nucleation of Co^{II}, Ni^{II}, and Fe^{III} centers on the T4 viral capsid without the use of any noble-metal catalyst to preactivate the virus. Direct growth and 3D organization of the Co, Ni, and Fe quantum particles on the bioscaffold is reported for the first time. We found that the peculiar conformation of the T4 capsid could play an important role in the nucleation of these metals.

[a] Dr. L. Hou, Prof. Dr. F. Gao, Dr. N. Li
Key Laboratory of Applied Chemistry
Yanshan University
Qinhuangdao 066004 (China)
Fax: (+86) 335-806-1569
E-mail: fmgao@ysu.edu.cn

Supporting information for this article is available on the WWW under http://dx.doi.org/10.1002/chem.201000393.

The T4 capsid is an elongated icosahedron and consists of a chemically functionalized surface associated with a regular pattern of four kinds of coat proteins: gp23*, gp24*, highly antigenic outer capsid (hoc), and small outer capsid (soc).[8] The capsid proteins all show protrusion characteristics with a fixed distance between two neighbors and form a repeated hexagonal lattice conformation on the surface (Figure 1a). By introducing nucleation centers to the active sites of these regular patterned proteins through using the interactions of covalent bonding or electrostatic attraction between the metal ions and the well-defined chemical groups inherent in proteins, allows us to exquisitely control the growth and positioning of the metal particles.[9] The natural dispersed configuration of available binding sites prevent the formation of large aggregates, which is favorable for assembling the 3D monodispersed particle array. The protrusion structure also has a steric-confinement effect on the growth of the metal particles, which is favorable for controlling the particle size. However, the protrusions could not be identified in the TEM investigation, instead a relatively smooth surface is observed (Figure 1b), thus avoiding confusion with the assembled metal particles. The surface chemistry of the T4 capsid coupled with the high chemical and physical stability of the protein assembly (i.e., stable up to 60 °C and at pH 5–9.5) provide an ideal bioscaffold for the site-specific nucleation of a variety of inorganic materials.

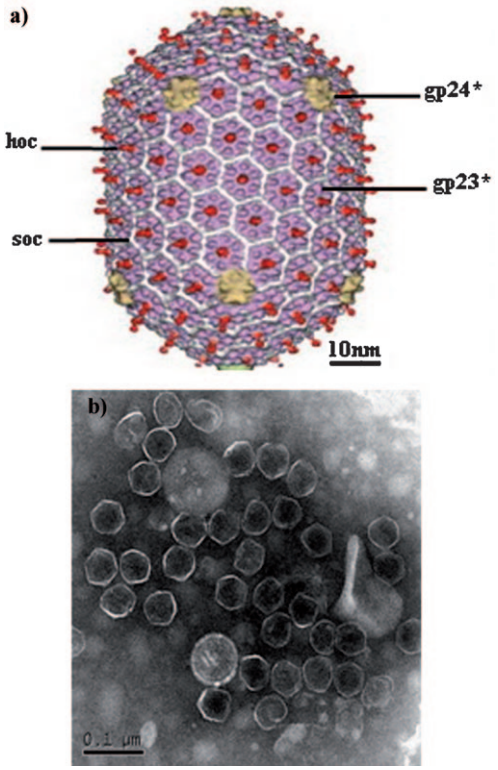

Figure 1. Structure of the T4 phage capsid. a) Model of the previously proposed T4 head structure. Proteins: gp23* = purple, gp24* = yellow, soc = white, hoc = red. b) TEM image of the collected wild-type T4 virions. JEM-2010 electron microscope operated at 200 kV and phosphotungstic acid was used as a negative stain.

Results and Discussion

We conducted the growth and 3D assembly of a series of metal quantum particles (e.g., Pt, Rh, Pd and Fe, Co, Ni) on the T4 capsid by using a nucleation-site control approach. The synthetic process comprises two major steps: First, the metal ions were introduced to specific functional groups on the T4 capsid by incubating T4 virions in a solution of a metal salt for several cycles (Scheme 1). Different biosorption mechanisms were operating during the process according to the specific interactions between the different chemical groups and metal ions. Second, a reductant was added to the incubated-virus suspension for the chemical reduction of the cationic M/V precursors. Prior to reduction, centrifugation to decrease the amount of the unbound metal ions in solution is necessary for the nucleation-site control for a small

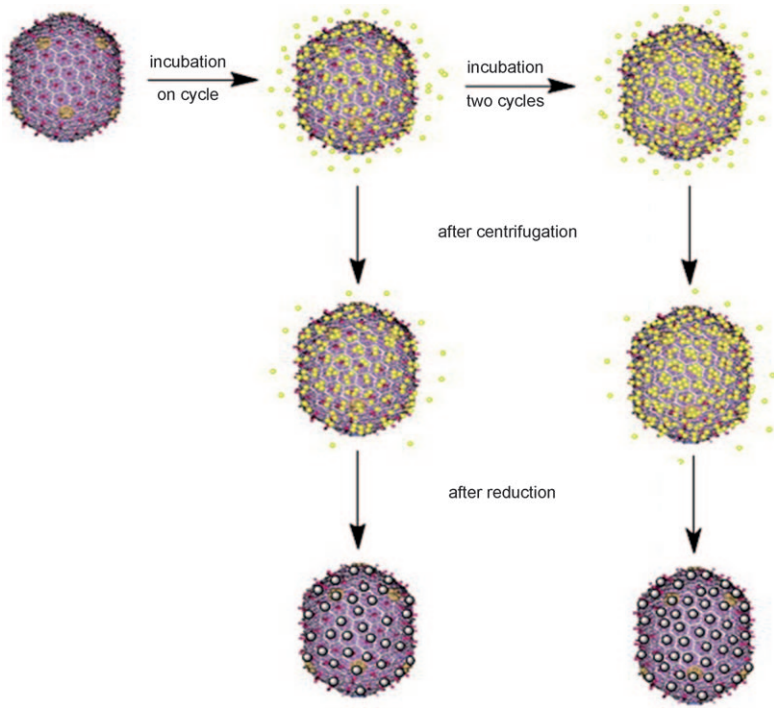

Scheme 1. Synthetic process of 3D patterned metal particles on a T4 capsid. The metal ion is shown in light yellow and the metal particle is shown in gray.

ratio of free/bound metal ions, which allows the reduction and nucleation of the primary particles to occur preferentially on the binding sites of the T4 capsid rather than in solution. That is to say, the prebound metal ions may form a nucleus with the nearest-neighbor ions adsorbed on the viral capsid after addition of the reductant, thus acting as deposition sites for further particle growth. Because there are not many free metal ions around the virions under these conditions, only a few metal ions can access the growing nucleus and form small particles. In comparison with previous proposals, this strategy provides a higher efficiency in the preparation of metal nanoparticles that were patterned in a monodispersed configuration on a viral capsid. Furthermore, the coverage density of the particles can be tuned simply by changing the incubation time or cycles of the virions in a solution of the metal salt.

We first choose Pt, Rh, and Pd as models in this study for several reasons. Protocols for solution synthesis by chemical reduction in which various biostructures, such as DNA, proteins, or viruses, were used as scaffolds for direct assembly have been reported.[10] The ordered noble-metal nanoparticle arrays are expected to serve as useful model systems for studying the effects of surface structure on catalyst performance in industrially important applications.[11] The synthesis of the well-ordered particle arrays requires initiation by seeding metal ions to specific functional groups of the virus protein surface. According to the Pearson concept,[12] Pt^{IV}, Rh^{III}, or Pd^{II} centers are soft metal ions and should tightly bind to the soft S-containing amino acids.[10b] For example, cysteine and methionine, typical components of gp23*, gp24*, and hoc, are situated outside the T4 virus capsid, and can thus act as S-donor ligands to complex with precious metal ions. By incubating the T4 virions in an aqueous solution of the metal chloride at neutral pH for several cycles and treating the system with dimethylaminoborane (DMAB) as a reductant, a range of M/V nanostructures with different coverage densities were obtained. TEM analysis allowed a large number of the assembled M/V nanostructures to be visualized (see Figure S1 in the Supporting Information), and high-magnification images revealed detailed structures of these complexes (Figure 2). The T4 virion can be seen as the deep-gray spherical structure, and the dark spots dispersed on and around the core are small metal particles. The patterned noble-metal nanoparticles are spheroidal and 3.0–4.5 nm in diameter, and the nearest neighbor distance (center point to center point) varies between 5 and 10 nm. The corresponding selected-area electron diffraction (SAED) patterns (inset in Figure 2a and Figure S2 in the Supporting Information) exhibit a typical ring character of crystalline nanoparticles, which can be indexed as Pt, Rh, or Pd metal centers with a face-centered cubic (fcc) structure. The uniform small size and monodispersed configuration confirms the high efficiency of the T4 template in the nucleation and stabilization of the noble-metal particles. When the Pt ions were reduced with DMAB under the same conditions but without the T4 template being present, no dispersive nanoparticles were obtained, instead large Pt agglomerates were finally formed in solution (see Figure S3 in the Supporting Information).

The metal-nanocrystal coverage density increases with a longer incubation time or more incubation cycles due to the

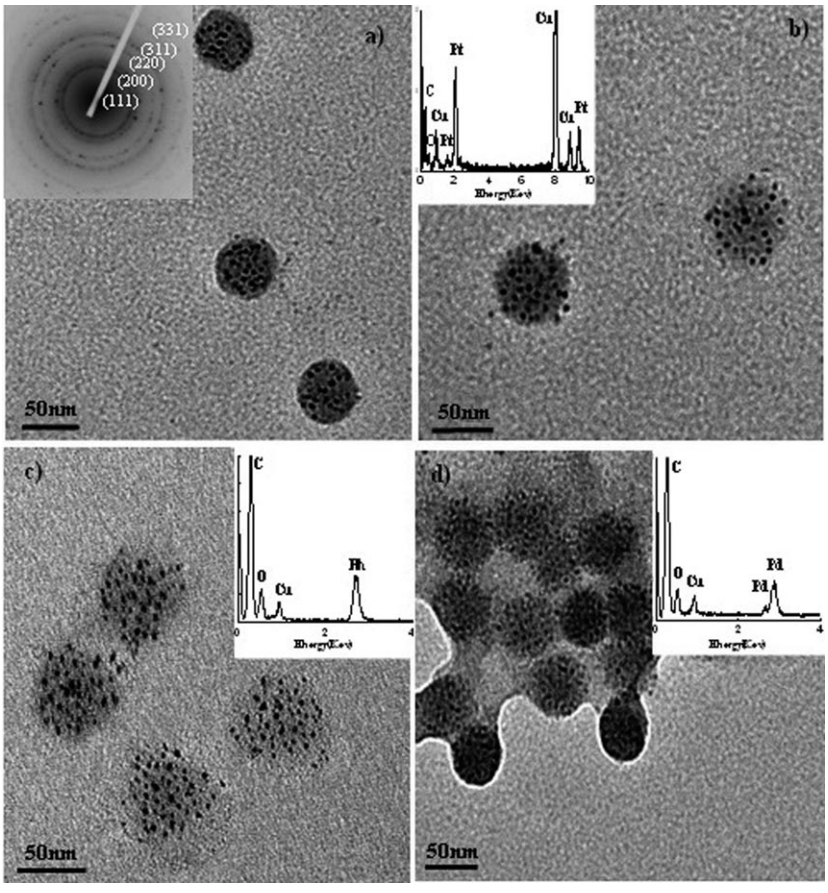

Figure 2. TEM images showing the T4 capsid covered by noble-metal nanoparticles. a) A Pt/T4 structure obtained through one incubation cycle of 24 h. Selected-area electron diffraction (SAED) pattern (inset) of a Pt nanoparticle on a viral capsid. b) A Pt/T4 structure obtained through two incubation cycles. c) Rh/T4 and d) Pd/T4 structures obtained through three incubation cycles. Inset: the corresponding energy-dispersive X-ray (EDX) spectra confirm the assembled particles on the viral capsid are made of pure Pt, Rh, and Pd, respectively.

larger number of nucleation seeds for metal-nanocrystal growth. For example, when the T4 virions were incubated in an aqueous solution of $PtCl_4$ for 6 h, the coverage density of the Pt particles was only 18% by area after reduction with DMAB (see Figure S4 in the Supporting Information), whereas it increased to 30% as the incubation time was prolonged to 20 h. During the on-going incubation, the increase in the coverage density of the Pt nanocrystals became slower and slower due to the decrease of free metal ions in solution. No further obvious change was observed over 24 h. When the collected T4 virions with bound metal ions were redispersed in a new aqueous solution of $PtCl_4$, the increase in the concentration of the free metal ions supplied a greater chance for the metal ions to bind to the rest of the active sites on the viral capsid. In comparison to the samples in Figure 2a, b, it can be clearly seen that the coverage density of the Pt particles on the T4 capsid increased with more cycles of the incubation process. These results demonstrate that the coverage density of nanocrystals on a viral capsid can be controlled simply by adjusting the incubation time and number of cycles. It is worth noting that after the last cycle of the incubation process, centrifugation should be carried out to remove most of the free metal ions around the virions, otherwise the patterned array of discrete nanoparticles can not be obtained, instead a complete metal coating was found over the whole capsid (see Figure S5 in the Supporting Information). This observation confirms the validity of the strategy to separate the incubated virions from the highly concentrated solution of the metal salt, thus avoiding growth in size and the coalescence of metal particles during reduction.

As a further example of the general use of this method, a similar approach was applied to the organization of Fe, Co, and Ni nanoparticles on the T4 viral capsid. In contrast to the Pt^{IV}, Rh^{III}, and Pd^{II} ions, Fe^{III}, Co^{II}, and Ni^{II} ions can not be stabilized by an organic ligand, which was demonstrated as no metal precipitate formed on the exterior surface of the capsid when the virions were treated with the same procedure as employed in the above-mentioned cases. To ensure sufficient affinity of ions to the surface, the collected virions had to be pretreated at a specially selected pH value (pH 8–9) for several hours because alkaline conditions usually create negatively charged groups (such as carboxylic groups) on the exterior of the capsid surface, which is favorable for metal cation binding by electrostatic interactions.[2,13] After incubation of the as-treated virions in an aqueous solution of the metal chlorides for two cycles and treatment with the reductant DMAB, a large number of complex M/V structures were found by TEM observation (see Figure S6 in the Supporting Information). High-magnification images (Figure 3) reveal that lots of dark spots with diameters of 2–4 nm were patterned over the whole viral capsid surface. The corresponding X-ray diffraction patterns and X-ray photoelectron spectra (see Figures S7 and S8 in the Supporting Information) confirm the dark spots are zero-valent metal crystallites, thus existing as Fe^0, Co^0, and Ni^0, respectively. No impurities such as metal oxides or precursor compounds were detected, and the broad reflection peak at around 22° might originate from the T4 macromolecules contained in the samples. The mean diameter of the organized metal particles, estimated from the XRD diffraction patterns by means of the Debye–Scherrer equation is about 3.8 nm (SD $\pm$ 1.0 nm), which is comparable to the analytical result (2–4 nm) obtained from several hundreds of counted metal particles from the representative TEM images (Figure 3). Based on the TEM image, the total population of the patterned metal particles analyzed is between 200 and 300 particles for each M/V structure, thus suggesting a high particle coverage of the capsid surface that reaches up to 65% in most cases. Although the number of assembled particles is large, metal nanoparticles do not distribute randomly, but locate at specific sites with high monodispersity, thus confirming the template-directed mechanism of the virus.

The growth of Ni and Co on or inside the tobacco mosaic virions (TMVs) has been previously reported, but only took place on an appropriate metal catalyst surface.[7a,b] As revealed by Knez et al.,[7a,b] pretreatment of the virion with

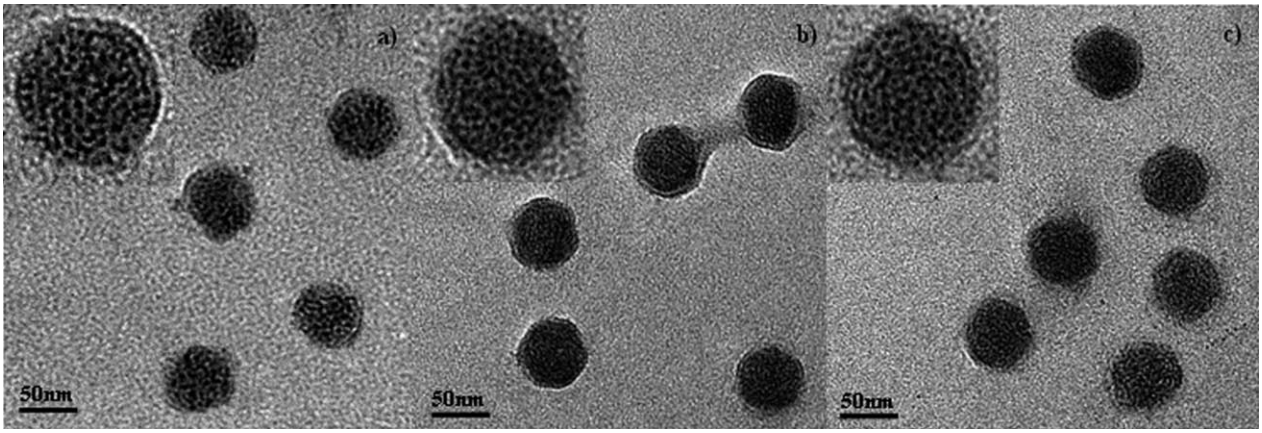

Figure 3. TEM images showing the T4 capsid covered by magnetic metal nanoparticles. a) Fe/T4, b) Co/T4, and c) Ni/T4 structures obtained through two incubation cycles. Inset: high-magnification TEM images that show the detailed structure of the M/V complexes.

Pd^{2+} or Pt^{2+} ions is necessary for the deposition of Ni and Co, namely, no metallization was obtained without activation. However, in this study, nucleation of Ni and Co occurred on the binding sites of a T4 viral capsid that had not been activated with any metal catalyst. To the best of our knowledge, similar investigations have been carried with the T7 phage as a template, but the nucleation and growth of Co nanoparticles has taken place only inside the empty capsid of the virus.[14] These observations suggest that the peculiar structure of the T4 capsid may play an important role in nucleation of the magnetic quantum particles. Presumably, the inherent protrusions on the exterior capsid surface may induce the attached metal ions to grow into small nuclei after adding the reductant. Because Ni and Co centers are themselves good catalysts, once the initial nucleus is obtained growth proceeds autocatalytically. This speculation may rely on the fact that when Co^{II} and Ni^{II} ions were reduced with DMAB under the same conditions, but without the T4 virions being present no metal nanocrystals were obtained.

These series of experiments present the successful synthesis and organization of metal particles on the T4 capsid with a high monodispersed configuration and small size distribution. Such organized nanoblocks are expected to show excellent performance in their application domains. It is well known that the specific activity of noble-metal catalysts is strongly related to their size, distribution, and support, thus highly dispersed catalyst nanoparticles of a small size and narrow size distribution are ideal for high electrocatalyst activity owing to their large surface-to-volume ratio.[15] The electroactive surface areas determined from CO-stripping voltammograms were 89.3, 241.2, and 133.1 $m^2 g^{-1}$ for the assembled Pt, Rh, and Pd nanocrystals, respectively (Figure 4a). In comparison with the tested value of the unsupported Pt particles (29.4 $m^2 g^{-1}$), which were synthesized without the assistance of any template, the electrocatalytic activity of the patterned noble-metal catalysts was clearly enhanced. High electrocatalytic activity is a beneficial feature of the complex noble metal/virus structures, which makes them promising for electrocatalytic applications, such as fuel cells.[16]

The magnetic properties of the resultant magnetic metal/virus structures were also investigated. For the most important ferromagnetic materials, it is known that Fe, Co, and Ni nanoparticles below 20 nm are in the superparamagnetic regime.[6] Although in our study, only the Ni/T4 structures showed superparamagnetic characteristics, with the saturation moment reaching 30.4 emu g^{-1}, samples of the Fe/T4 and Co/T4 structures still exhibit ferromagnetic behavior, including coercivity (H_C) and remanence (M_R). As reported previously, Fe nanoparticles 7.0 nm in diameter also showed good ferromagnetic behavior when patterned in a thin film array with interparticle spacing of 2.5 nm.[17] Reasons for this behavior may be due to the fact that, as opposed to bulk materials, the magnetic interactions in nanoparticle arrays are determined not only by particle size but particle separation. It can be seen in Figure 4b with enlargement

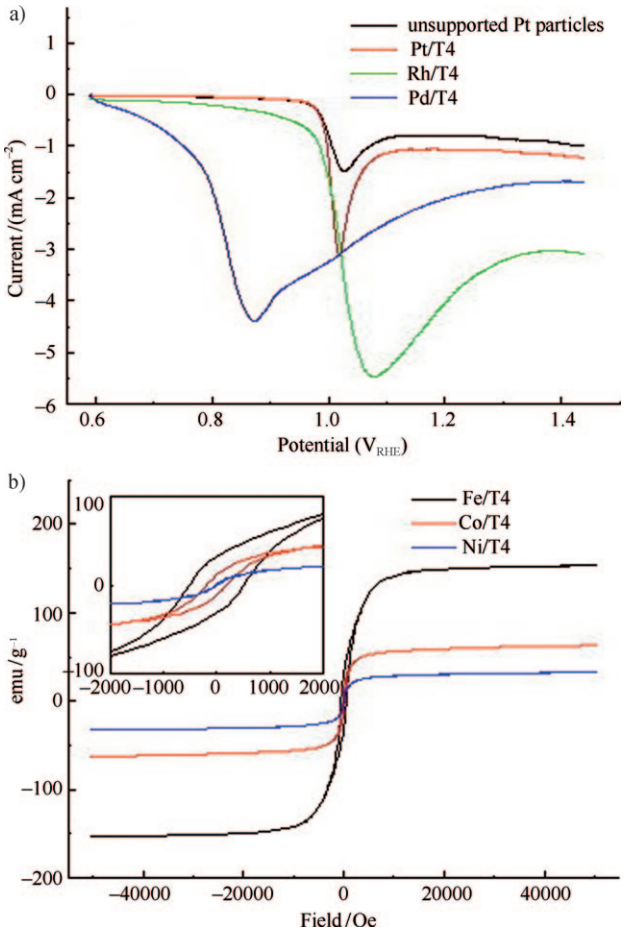

Figure 4. a) CO-stripping voltammogram for the unsupported Pt nanoparticles and samples of Pt/T4, Rh/T4, and Pd/T4 obtained via two incubation cycles. b) Hysteresis loop at 100 K for the samples of Fe/T4, Co/T4, and Ni/T4. Inset: low-field region of the hysteresis loop.

near the origin that the saturation magnetization (M_S) of the Fe/T4 structure could be determined to be 151.1 emu g^{-1}, which is less than in bulk iron (218 emu g^{-1}) but significantly higher than the corresponding metal oxide (Fe_3O_4; 80 emu g^{-1}). The stable complex M/V structures with high magnetic moments are predicted to have important applications in biosensing, drug delivery, and magnetic resonance imaging (MRI) contrast enhancement.

Conclusion

In conclusion, the direct synthesis and 3D organization of quantum-size Pt, Rh, Pd, Fe, Co, and Ni particles on a viral capsid were achieved simply by incubating T4 virions in a solution of the metal salt and treating with a reductant. Different chemical groups inherent in on the capsid protein were used as ligands or to electrostatically bind metal ions. Centrifugation to decrease the unbound metal ions around the virions was carried out to ensure the reduction and nucleation of metal ions occurred mainly on the binding sites. The growth of metal particles in situ yielded a highly dis-

persed configuration and a small size distribution, which are properties that contributed to high electrocatalytic activities of the obtained noble metal particles. Also, the coverage density of particles could be tuned simply by changing the incubation time or cycles of the virions. We believe this simple fabrication method by means of a T4 bioscaffold can be applied to various metals and semiconductors to produce inorganic particle/virus composites with interesting materials properties. These perspectives are currently being explored in our laboratory.

Experimental Section

Collection of T4 virions: To produce abundant T4 virions, a concentrated crude lysate of wild-type bacteriophage T4 was multiplied on *E. coli* B cells by using a lysogeny broth (LB) medium (both strains of the bacteria and virus were purchased from the Wuhan Institute of Virology, Chinese Academy of Science). The collection and purification of the T4 virions was described in detail previously.[18] The purified virions were stored in deionized water for further use. To avoid the influence of the tail on the adsorption of metal ions, virions were processed to contract the tails. A sample of the T4 phage (1 mL) was diluted tenfold by using urea (3 M) buffered with tris(hydroxymethyl)aminomethane (Tris) HCl (50 mM) at pH 8.0, complemented with $MgCl_2$ (1 mM), and incubated for 2 h at 4 °C The sample was further diluted threefold and centrifuged for 2.5 h at 110000 *g* and 4 °C in a Beckman SW41Ti rotor. The resulting pellet was dissolved slowly in deionized water (500 μL).

Synthesis and organization of noble-metal particles on T4 capsid: Three portions of the stock T4 suspension (250 μL) were mixed with an aqueous solution of $PtCl_4$ (500 μL, 10 mM), an aqueous solution of $RhCl_3$ (500 μL, 10 mM), or a saturated solution of $PdCl_2$, respectively. The mixtures were vortically agitated for 5 min, followed by several hours incubation at 6 °C. The incubation time was varied to control the density of the metal ions on the T4 capsid between 6 and 24 h. The systems were diluted tenfold with deionized water and centrifuged at 110000 *g* for 2.5 h. The supernatant was removed and the pellet was dispersed in the same amount of solution of the metal salt for reincubation and repeated centrifugation. This process was repeated 1–3 times to obtain a series of metal ion/virus composites with different coverage densities. After the last centrifugation process, most of supernatant was removed, leaving only 400 μL to dissolve the pellet. The systems were reduced by the dropwise addition a solution of dimethylaminoborane in water (DMAB; 10 mM). The obtained samples were kept at 6 °C for further investigation.

Synthesis and organization of magnetic metal particles on T4 capsid: Three portions of the stock T4 suspension (400 μL) were maintained at pH 8.5–9 for 4 h and mixed with a freshly prepared aqueous solution of $FeCl_3$, $CoCl_2$, or $NiCl_2$ (500 μL, 10 mM), respectively. The mixtures were vortically agitated for 5 min, followed by incubation for 24 h at 6 °C. The systems were diluted tenfold with deionized water and centrifuged at 110000 *g* for 2.5 h. The supernatant was removed and the pellet was dispersed in the same amount of solution of the metal salt for another cycle of the incubation After the last centrifugation process, most of the supernatant was removed, thus leaving only 400 μL to dissolve the pellet. The systems were reduced by the dropwise addition of an aqueous solution of DMAB (10 mM). To avoid oxidation of the assembled magnetic metal particles, which was caused by exposure to air, the reaction solution was purged with highly pure nitrogen immediately after adding the reductant for 0.5 h. The sample was sealed in an Eppendorf tube (2 mL) under a nitrogen atmosphere and kept at 6 °C for further investigation.

TEM studies: TEM analysis of the samples was made on a JEM-2010 electron microscope operated at 200 kV and equipped with an energy-dispersive X-ray (EDX) analyzer. Typically droplets of a suspension (5–10 uL) were deposited on carbon-coated 300 mesh copper grids. Excess water was removed with filter paper and the preparation for magnetic metal/virus samples was nitrogen-dried. Phosphotungstic acid (2 wt%, pH 6.8) was used as a negative stain for better observation of the collected pure T4 virions.

X-ray powder diffraction studies: XRD measurements of magnetic metal/virus samples were carried out on a D/max-2500/PC X-ray diffractometer with a graphite monochromator using $Cu_{K\alpha}$ radiation (λ = 0.15418 nm) to study the phases in situ. Prior to the experiment, the as-prepared M/V suspensions were freeze dried in vacuo at −100 °C to collect enough dry powder for XRD analysis. A glass substrate that held the powder sample was covered by adhesive tape on the surface to prevent the sample from exposure to air during the measurements. The scan data were collected in the 2θ range of 10–90° with a step size of 2° min^{-1}.

The dry powders were sealed in an Eppendorf tube (1.5 mL) under nitrogen for protection to ensure the samples remain unoxidized during shipping for XRD, X-ray photoelectron spectroscopy (XPS), and the characterization of magnetic properties.

XPS studies: Measurement of XPS spectra was carried out on an ECSA-LAB 250 X-ray photoelectron spectrometer with an $Al_{K\alpha}$ X-ray source (15 kV, 1500 W) to analyze the valence states of the patterned magnetic metals on the viral capsid. The Ar^+ sputtering was carried out under the following conditions: background vacuum = 2.2×10^{-7} Pa, sputtering time = 1.5 min. The binding energies obtained in the XPS analysis were calibrated against the C1s peak at 284.6 eV. The test powder samples were prepared by using the same method as for XRD analysis.

Magnetic studies: A superconducting quantum interference device (SQUID, Quantum Design MPMS-XL-7) magnetometer was used to measure the magnetic properties of the T4 assemblies of the Fe, Co, and Ni nanoparticles. This system can detect magnetic moments in the range of 10^{-9} to 1 emu with good signal/noise ratios. The hysteresis loops were recorded at 100 K and a magnetic field up to 50 KOe. The sample was set up in a glovebox with nitrogen by packing the powder samples with plastic wrap and fixing in a plastic tube. The powder samples were prepared by using the same method as for XRD analysis.

Electrochemical experiments: Electrochemical experiments were performed by using the thin-film voltammetric techniques developed by Schmidt et al.[19] Prior to the experiment, the quality score of assembled noble-metal particles was confirmed: An obtained M/V suspension was freeze-dried at −100 °C to provide a given amount of dry powder, the weight was carefully measured to an accuracy of ±0.01 mg, the powders were calcinated at 400 °C for 1 h to remove the T4 template and other organic impurities, and the weight of the obtained pure noble-metal particles was measured to calculate its quality score.

The working electrode was prepared by making aqueous slurries of the dried T4-supported noble-metal powder with concentrations of 0.5–2.5 g L^{-1}. Multiple slurries were prepared to estimate uncertainties in the sample-preparation procedures and the experimental measurements. A glassy carbon electrode (GCE; diameter = 4 mm, area = 0.1257 cm^2) was polished with electrochemical-grade alumina paste and sonicated in methanol prior to the deposition of the catalyst powder. The aqueous slurries were sonicated for a minimum of 30 min. A drop of the sonicated slurry (5 μL) was deposited onto the cleaned GCE. The catalyst was allowed to dry before a thin-layer coating (ca. 0.5 μm) of Nafion was applied (5 wt% in methanol further diluted 1:10 in methanol). The resulting catalyst loadings were between 1 and 6 μg of noble-metal particles.

A standard three-electrode cell was employed with a SCE as the reference electrode, a Pt foil as the counterelectrode, and the catalyst-coated GCE as the working electrode (WE). All the potentials are referenced to a reversible hydrogen electrode (RHE). CO-stripping experiments were performed at laboratory temperature (20–22 °C). Prior to all the voltammetric experiments, each catalyst was electrochemically conditioned in H_2SO_4 (0.5 M) by briefly (5–10 s) polarizing the WE to potentials at which hydrogen evolution occurs (i.e., less than 0 mV_{RHE}).

In the CO-stripping measurements, the evolved hydrogen was removed from the WE by rotating the electrode and CO was adsorbed onto the electrocatalyst surface by holding the potential at 100 mV_{RHE} for 6 min in H_2SO_4 (0.5 M) saturated with ultrahigh purity (UHP) CO. This procedure was carried out while rotating the WE at 1000 rpm to increase mass

transfer. The potential was swept at $20\,mV\,s^{-1}$ from 600 to $1440\,mV_{RHE}$. Five separate electrodes for the catalyst were tested, thus resulting in five separate measurements to determine average values and standard deviations. Representative CO-stripping voltammograms are shown in Figure 4, and the procedures used in the calculation of the electroactive surface areas are described below. The Pt catalyst was taken as an example.

The peak at about $1024\,mV_{RHE}$ is attributed to current being passed as CO adsorbed on the electroactive Pt surface (Pt–CO) is stripped away from the surface (oxidized) according to the reaction given in Equation (1).

$$Pt-CO + H_2O \rightarrow CO_2 + 2H^+ + 2e^- \quad (1)$$

The exact shape and position of the peak changes but is not significant in this study, as the parameter of interest is the charge Q that results from the CO oxidation event. The charge is calculated by integrating the background-subtracted current as a function of time. Q is plotted versus Pt loading. If the data are fit with a linear regression with a zero intercept, the electroactive surface area ($SA_{e\text{-active}}$) can be calculated from Equation (2),

$$SA_{e\text{-active}} = 1000 \cdot \text{slope} \cdot N_A/F \cdot XSA_{Pt}/n \quad (2)$$

where the slope is in units of $mC\,\mu gPt^{-1}$, N_A = Avogadro number (6.022×10^{23} atoms mol^{-1}), F = Faraday constant ($96\,486\,C\,mol^{-1}$), XSA_{Pt} = atomic cross-sectional area of a Pt atom ($8.00 \times 10^{-20}\,m^2\,atom^{-1}$), n = number of electrons in the CO oxidation reaction ($2e^-$), and 1000 is a metric conversion factor. The value for $SA_{e-active}$ is reported in the text.

Acknowledgements

The authors acknowledge the financial support from the National Natural Science Foundation of China (No. 50672080) and the Foundation for the Author of National Excellent Doctoral Dissertation of PR China (No. 200434). L.H. acknowledges the financial support from the Science Foundation of Yanshan University for the Excellent Ph.D. students.

[1] a) T. Douglas, M. Young, *Nature* **1998**, *393*, 152–155; b) C. E. Fowler, W. Shenton, G. Stubbs, S. Mann, *Adv. Mater.* **2001**, *13*, 1266–1269; c) M. Allen, D. Willits, M. Young, T. Douglas, *Inorg. Chem.* **2003**, *42*, 6300–6305; d) N. Ma, C. J. Dooley, S. O. Kelley, *J. Am. Chem. Soc.* **2006**, *128*, 12598–12599; e) L. Berti, A. Alessandrini, P. Facci, *J. Am. Chem. Soc.* **2005**, *127*, 11216–11217; f) S. R. Hall, W. Shenton, H. Engelhardt, S. Mann, *ChemPhysChem* **2001**, *2*, 184–186; g) S. Balci, K. Noda, A. M. Bittner, A. Kadri, C. Wege, H. Jeske, K. Kern, *Angew. Chem.* **2007**, *119*, 3210–3212; *Angew. Chem. Int. Ed.* **2007**, *46*, 3149–3151.

[2] E. Dujardin, C. Peet, G. Stubbs, J. N. Culver, S. Mann, *Nano Lett.* **2003**, *3*, 413–417.

[3] M. Okuda, Y. Kobayashi, K. Suzuki, K. Sonoda, T. Kondoh, A. Wagawa, A. Kondo, H. Yoshimura, *Nano Lett.* **2005**, *5*, 991–993.

[4] Q. Wang, T. W. Lin, L. Tang, J. E. Johnson, M. G. Finn, *Angew. Chem.* **2002**, *114*, 477–480; *Angew. Chem. Int. Ed.* **2002**, *41*, 459–462.

[5] a) A. S. Blum, C. M. Soto, C. D. Wilson, J. D. Cole, M. Kim, B. Gnade, A. Chatterji, W. F. Ochoa, T. W. Lin, J. E. Johnson, B. R. Ratna, *Nano Lett.* **2004**, *4*, 867–870; b) A. S. Blum, C. M. Sota, C. D. Wilson, T. L. Brower, S. K. Pollack, T. L. Schull, A. Chatterji, T. Lin, J. E. Johnson, C. Amsinck, P. Franzon, R. Shashidhar, B. R. Ratna, *Small* **2005**, *1*, 702–706; c) W. Chen, A. Bian, A. Agarwal, L. Liu, H. B. Shen, L. B. Wang, L. N. Xu, A. Kotov, *Nano Lett.* **2009**, *9*, 2153–2159.

[6] S. Peng, C. Wang, J. Xie, S. H. Sun, *J. Am. Chem. Soc.* **2006**, *128*, 10676–10677.

[7] a) M. Knez, M. Sumser, A. M. Bittner, C. Wege, H. Jeske, T. P. Martin, K. Kern, *Adv. Funct. Mater.* **2004**, *14*, 116–124; b) M. Knez, A. M. Bittner, F. Boes, C. Wege, H. Jeske, E. Mai, K. Kern, *Nano Lett.* **2003**, *3*, 1079–1082; c) R. kirsch, M. Mertig, W. Pompe, R. Wahl, G. Sadowski, K. J. Bohm, E. Unger, *Thin Solid Films* **1997**, *305*, 248–253.

[8] a) A. Fokine, P. R. Chipman, P. G. Leiman, V. V. Mesyanzhinov, V. B. Rao, M. G. Rossmann, *Proc. Natl. Acad. Sci. USA* **2004**, *101*, 6003–6008; b) Q. Li, S. B. Shivachandra1, S. H. Leppla, V. B. Rao, *J. Mol. Biol.* **2006**, *363*, 577–588.

[9] a) W. Shenton, T. Douglas, M. Young, G. Stubbs, S. Mann, *Adv. Mater.* **1999**, *11*, 253–256; b) E. Gillitzer, D. Willits, M. Young, T. Douglas, *Chem. Commun.* **2002**, 2390–2391; c) C. A. Mirkin, R. L. Letsinger, R. C. Mucic, J. J. Storhoff, *Nature* **1996**, *382*, 607–609.

[10] a) M. Mertig, L. Colombi, R. Seidel, W. Pompe, *Nano Lett.* **2002**, *2*, 841–844; b) S. Behrens, K. Rahn, W. Habicht, K. J. Bohm, H. Rosner, E. Dinjus, E. Unger, *Adv. Mater.* **2002**, *14*, 1621–1625; c) Y. Hatakeyama, M. Umetsu, S. Ohara, F. Kawadai, *Adv. Mater.* **2008**, *20*, 1122.

[11] a) S. S. Mark, M. Bergkvist, X. Yang, E. R. Angert, C. A. Batt, *Biomacromolecules* **2006**, *7*, 1884–1887; b) J. Zhu, G. A. Somorjai, *Nano Lett.* **2001**, *1*, 8–13.

[12] a) R. G. Pearson, *J. Am. Chem. Soc.* **1963**, *85*, 3533–3543; b) R. Parr, R. G. Pearson, *J. Am. Chem. Soc.* **1983**, *105*, 7512–7516.

[13] A. V. Pethkar, S. K. Kulkarni, K. M. Paknikar, *Bioresour. Technol.* **2001**, *80*, 211–215.

[14] C. Liu, S. H. Chung, Q. L. Jin, A. Sutton, F. Yan, A. Hoffmann, B. K. Kay, S. D. Bader, L. Makowski, L. H. Chen, *J. Magn. Magn. Mater.* **2006**, *302*, 47–51.

[15] Y. J. Song, Y. Yang, C. J. Medforth, E. Pereira, A. K. Singh, H. F. Xu, Y. B. Jiang, C. J. Brinker, F. V. Swol, J. A. Shelnutt, *J. Am. Chem. Soc.* **2004**, *126*, 635–645.

[16] G. W. Zhao, J. P. He, C. Zhang, X. J. Zhou, H. X. Chen, T. Wang, *J. Phys. Chem. A* **2008**, *112*, 1028–1033.

[17] D. Farrell, Y. H. Cheng, R. W. McCallum, M. Sachan, S. A. Majetich, *J. Phys. Chem. A* **2005**, *109*, 13409–13419.

[18] a) L. W. Black, .D. T. Brown, *J. Virol.* **1976**, *17*, 894–904; b) K. Asami, X. H. Xing, Y. Tanji, H. J. Unno, *Ferment. Bioeng.* **1997**, *83*, 511–516.

[19] T. J. Schmidt, H. A. Gasteiger, G. D. Stab, P. M. Urban, D. M. Kolb, R. J. Behm, *J. Electrochem. Soc.* **1998**, *145*, 2354–2358.

Received: February 13, 2010
Revised: May 14, 2010
Published online: November 18, 2010

